Journal of Colloid and Interface Science 650 (2023) 883–891

Contents lists available at ScienceDirect

Journal of Colloid And Interface Science

journal homepage: www.elsevier.com/locate/jcis

Electrostatic interactions control the adsorption of extracellular vesicles onto supported lipid bilayers

Andrea Ridolfi [a,b,*], Jacopo Cardellini [b,c], Fatlinda Gashi [d], Martijn J.C. van Herwijnen [e], Martin Trulsson [f], José Campos-Terán [g,h], Marca H. M. Wauben [e], Debora Berti [b,c], Tommy Nylander [d,h,i], Joakim Stenhammar [d,*]

[a] Department of Physics and Astronomy and LaserLaB Amsterdam, Vrije Universiteit Amsterdam, Amsterdam, the Netherlands
[b] Department of Chemistry "Ugo Schiff", University of Florence, Florence, Italy
[c] CSGI, Consorzio Sistemi a Grande Interfase, University of Florence, Sesto Fiorentino, Italy
[d] Division of Physical Chemistry, Lund University, Lund, Sweden
[e] Department of Biomolecular Health Sciences, Faculty of Veterinary Medicine, Utrecht University, Utrecht, the Netherlands
[f] Division of Computational Chemistry, Lund University, Lund, Sweden
[g] Departamento de Procesos y Tecnología, Universidad Autónoma Metropolitana-Cuajimalpa, México City, Mexico
[h] LINXS - Institute of Advanced Neutron and X-ray Science, Lund, Sweden
[i] NanoLund, Lund University, Lund, Sweden

GRAPHICAL ABSTRACT

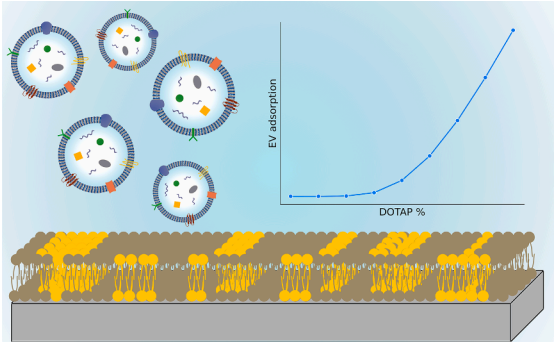

ABSTRACT

Communication between cells located in different parts of an organism is often mediated by membrane-enveloped nanoparticles, such as extracellular vesicles (EVs). EV binding and cell uptake mechanisms depend on the heterogeneous composition of the EV membrane. From a colloidal perspective, the EV membrane interacts with other biological interfaces via both specific and non-specific interactions, where the latter include long-ranged electrostatic and van der Waals forces, and short-ranged repulsive "steric-hydration" forces. While electrostatic forces are generally exploited in most EV immobilization protocols, the roles played by various colloidal forces in controlling EV adsorption on surfaces have not yet been thoroughly addressed. In the present work, we study the adsorption of EVs onto supported lipid bilayers (SLBs) carrying different surface charge densities using a combination of quartz crystal microbalance with dissipation monitoring (QCM-D) and confocal laser scanning microscopy (CLSM). We demonstrate that EV adsorption onto lipid membranes can be controlled by varying the strength of electrostatic forces and we theoretically describe the observed phenomena within the framework of nonlinear Poisson-Boltzmann theory. Our modelling results confirm the experimental

* Corresponding authors.
E-mail addresses: a.ridolfi@vu.nl (A. Ridolfi), joakim.stenhammar@fkem1.lu.se (J. Stenhammar).

https://doi.org/10.1016/j.jcis.2023.07.018
Received 18 April 2023; Received in revised form 26 June 2023; Accepted 5 July 2023
Available online 6 July 2023

observations and highlight the crucial role played by attractive electrostatics in EV adsorption onto lipid membranes. They furthermore show that simplified theories developed for model lipid systems can be successfully applied to the study of their biological analogues and provide new fundamental insights into EV-membrane interactions with potential use in developing novel EV separation and immobilization strategies.

1. Introduction

Cell-to-cell communication is involved in many biological processes and in the onset and spread of multiple pathological conditions in multicellular organisms. Depending on the location, relative distance, and type of message to be delivered, cells can use several different communication pathways [1–2]. One of the most powerful strategies for long-distance communication between cells located in different parts of an organism is the production and secretion of membrane-enveloped nanoparticles [3–4], where one of the most intriguing classes is extracellular vesicles (EVs) [5–7]. EVs are unilamellar vesicles, typically in the nanometric range, used by cells as carriers for biological material such as proteins, carbohydrates and nucleic acids [8–9]. EV binding and fusion with, or uptake by, target cells occur via multiple different mechanisms. Many of them, such as vesicle fusion and raft- and receptor-mediated endocytosis, strongly depend on the heterogeneous composition of the EV membrane [10], which consists of a multicomponent lipid bilayer containing a wide range of membrane proteins and biomolecules [8].

From a colloidal perspective, the EV membrane can interact with other biological interfaces *via* both specific and non-specific interactions [3,11–12]. The latter category is typically dominated by electric double layer and van der Waals forces, as outlined in the DLVO theory of colloidal stability, and short-ranged repulsive "steric-hydration" forces of unclear molecular origin that have been measured between hydrated lipid bilayers [13–14]. Several studies have demonstrated that phenomena such as adsorption, deformation, and rupture of synthetic lipid vesicles in contact with charged substrates are strongly dependent on the magnitude of electrostatic interactions [15–17]. Moreover, electrostatic interactions are commonly exploited to adsorb and immobilize EVs and synthetic lipid vesicles on solid substrates to study their properties [18–21]. The most common setup to study the interaction of lipid vesicles with lipid membranes under controlled and simplified conditions consists of a supported lipid bilayer (SLB), *i.e.*, a planar lipid bilayer deposited onto a rigid support [22–25]. Recent investigations have specifically probed the interaction of biologically derived EVs with SLBs [26–27], however without addressing the roles of generic colloidal forces in controlling EV adsorption.

In the present work, we employ weakly negatively charged EVs derived from bovine milk as a model system to study EV adsorption on synthetic SLBs with varying positive surface charge densities. This setup enables us to study the specific roles played by electrostatics in the interactions between EVs and other charged lipid interfaces under controlled conditions. Even though most natural lipid membranes possess negative surface charge densities, we note that zwitterionic lipid surfaces, which are ubiquitous in Nature, can assume a positive net charge under physiologically relevant concentrations of divalent ions such as Ca^{2+} or Mg^{2+} [28–29]. To generate charge-controlled SLBs, we use mixed liposomes composed of zwitterionic 1,2-dioleoyl-*sn*-glycero-3-phosphocholine (DOPC) and cationic 1,2-dioleoyl-3-trimethylammonium-propane (DOTAP). Tuning the ratio between the two amphiphilic molecules allows us to accurately control the surface charge density of the SLBs. We quantified the adsorption of EVs on the SLBs using two independent experimental techniques: quartz crystal microbalance with dissipation monitoring (QCM-D) and confocal laser scanning microscopy (CLSM). The two characterization techniques independently demonstrate that EV adsorption onto lipid membranes can be readily controlled by varying the magnitude of the positive surface charge density of the SLB. For SLBs composed of less than 40% w/w of DOTAP, corresponding to low surface charge densities, EV adsorption is negligible. In contrast, for higher contents of cationic DOTAP molecules, EV adsorption increases monotonically with the DOTAP/DOPC ratio. Assuming electrostatics to be the main driver for EV adsorption, we rationalize the EV-SLB interactions within the framework of nonlinear Poisson-Boltzmann (PB) theory, which accurately describes the electrostatic interactions between unequally charged surfaces [30]. When the resulting interaction free energy curves are combined with empirically measured short-range forces known to act between lipid bilayers, they confirm that attractive electrostatic interactions are indeed expected to be the dominant driver of EV adsorption for the experimentally studied DOTAP/DOPC ratios. Our results furthermore show that, in spite of their molecular complexity, EV interactions can be accurately described using simple models traditionally used for simpler colloidal model systems.

2. Materials and methods

2.1. Liposome preparation for QCM experiments

1,2-dioleoyl-*sn*-glycero-3-phosphocholine (DOPC) and 1,2-dioleoyl-3-trimethylammonium-propane (DOTAP) dry powders were purchased from Sigma Aldrich (St. Louis, MO, USA). Different amounts of DOPC and DOTAP were used to tune the surface charge of the employed liposomes; Table S1 reports the DOTAP/DOPC w/w percentages employed in the study, together with the nomenclature used in the next sections to describe them. In general, to prepare liposomes, the amount of DOPC and DOTAP powders corresponding to the desired final composition were weighed in to yield a total mass of 40 mg, before being dissolved in chloroform. Chloroform was then gently evaporated using a stream of nitrogen, leaving a thin lipid film at the bottom of the vials. The vials were covered with aluminum foil and put into a vacuum chamber overnight to allow the lipid films to dry completely. The following day, the lipid films were hydrated using 4 ml of PBS and the dispersions were successively extruded using 200 nm NanoSizer MINI Liposome Extruder (T&T Scientific). The extruded liposome dispersions were further diluted with PBS to a final concentration of 0.25 mg/ml for the subsequent experiments.

2.2. EV isolation and purification

Raw bovine milk (100 ml) was collected from a cooled tank in a local dairy farm (Tolakker, Utrecht, The Netherlands), transferred to 50 ml polypropylene tubes and centrifuged for 10 min at 22°C at 3000*g* (Beckman Coulter Allegra X-12R, Fullerton, CA, USA). After removal of the cream layer, the milk supernatant was harvested without disturbing the pellet and transferred to new tubes. A second centrifugation step at 3000*g* followed, after which the milk supernatant was collected and stored at −80 °C until further processing. To isolate milk EVs, thawed milk supernatant was transferred to polyallomer SW40 tubes (Beckman Coulter) and centrifuged at 5000*g* for 30 min at 4 °C and subsequently at 10000*g* (Beckman Coulter Optima L-90K with a SW40Ti rotor). For the precipitation of caseins, the milk supernatant was acidified to pH 4.6 by adding hydrochloric acid (HCl, 1 M) while stirring. Caseins were pelleted by centrifugation at 360*g* (Beckman Coulter Allegra X-12R) for 10 min at 4 °C, after which casein-free milk supernatant was collected and neutralized to pH 7.0 with sodium hydroxide (NaOH 1 M). Next, 6.5 ml of the milk 10000*g* supernatant was loaded on top of a 60% – 10% Optiprep gradient (OptiprepTM, Progen Biotechnik GmbH, Heidelberg, Germany) made in a SW40 tube. Gradients were ultracentrifuged at 192,000*g* (Beckman Coulter Optima L-90K with a SW40Ti rotor) for

15 −18 h. After centrifugation, fractions of 500 μl were harvested and densities were measured to identify the EV-containing fractions (Density 1.06 −1.19 g/ml), which were pooled. Optiprep was removed during size exclusion chromatography of the pooled EV-containing fractions using a 20 ml column (Bio-Rad Laboratories, Hercules, CA, USA) packed with 15 ml Sephadex g100 (Sigma-Aldrich, St. Louis, MO, USA). Fractions of 1 ml were eluted from the column with PBS (GibcoTM, Invitrogen, Carlsbad, CA, USA). The EV-containing fractions 3 to 9 were pooled and stored at −80 °C until use. For all the adsorption experiments (QCM-D and CLSM), milk EV preparations were diluted 1:200. The procedure of bovine milk EV isolation, as well as the analysis of milk EV preparations by Colorimetric Nanoplasmonic Assay (CONAN), Atomic Force Microscopy (AFM) and by Western-blotting has been previously described [21] and reported in the EV-TRACK knowledgebase (EV190077).

2.3. DLS and ζ potential measurements

Dynamic light scattering (DLS) measurements were performed using a Zetasizer Nano ZS (Malvern Panalytical Ltd., Malvern, UK), yielding information about the size distribution of both liposomes and EVs. Measurements were performed in triplicate, each one comprising 7 runs of 30 s each. The same instrument was then used for measuring the ζ potential of the lipid vesicles; measurements were performed in triplicate and comprised 10 runs with automatic attenuation and optical settings for all samples. For both DLS and ζ potential, the measurements were performed in PBS at a constant temperature of 25 °C. The hydrodynamic radii of the vesicles are reported in Table S2, together with the respective autocorrelation functions and fits obtained from DLS analysis (Figure S1). The obtained results and error values are expressed as the average and standard deviation of the respective triplicate for each sample.

2.4. Nanoparticle tracking analysis

Purified bovine milk EV preparations were quantified by nanoparticle tracking analysis (NTA) according to the procedure described previously [31], employing a NanoSight NS300 instrument (Malvern Instruments Ltd, UK) equipped with a 405 nm laser and a high sensitivity sCMOS camera. The NanoSight NTA software (version 3.2.16) was used for data acquisition and processing. The EV sample was diluted in endotoxin-free Dulbecco's 1X PBS without Ca^{2+} and Mg^{2+} (TMS-012-A Millipore). Three technical replicates were measured in various dilutions ranging from 1:500 to 1:1000 in a 60-second video under controlled temperature set at 20° C.

2.5. QCM-D experiments

Quartz crystal microbalance with dissipation monitoring (QCM-D) experiments were performed using a Q-Sense E4 instrument (Biolin Scientific, Göteborg, Sweden) using silicon oxide coated 5 MHz AT-cut quartz crystal sensor chips (Biolin Scientific) as substrate for the vesicle deposition. Prior to each experiment, the sensor chips were sequentially immersed in Hellmanex 2%, Ethanol and MilliQ water under sonication in an ultrasonic bath for 7 min for each solvent. After being dried in a stream of nitrogen, the sensor chips were then further cleaned in an air plasma for 1 min at 0.02 mbar using a plasma cleaner (Harrick Scientific Corp, model PDC-3XG, New York, USA). The sensor chips were then immediately placed in the sealed QCM-D measurement chambers and buffer was flowed through the chamber. The temperature was fixed at 25°C and kept constant throughout all the experiments. During the QCM-D measurements, variations in both the resonance frequency and energy dissipation of the sensor chips were recorded as a function of time. All the vesicle (liposome and EV) injection and buffer exchange steps were performed using a flow rate of 0.8 ml/min. To form the SLBs, liposomes were flushed within the QCM-D measurement chamber, where they adsorbed on the sensor surface. Then, MilliQ water was flushed to create an osmotic imbalance and promote the rupture of still intact liposomes. Once the whole sensor surface was covered with SLBs, indicated by a frequency drop of 20 −30 Hz and negligible change in dissipation, the buffer was changed to PBS and the systems were left to equilibrate for approximately 1 h. As can be seen from the traces in Figure S3, the signals describing the SLB formation remain stable after replacing the buffer solution, confirming the stability of SLBs under all the studied conditions. After SLB equilibration, the EV solution was injected in the QCM-D chamber. The outlet solution was collected and re-injected within the QCM-D chamber three times, to maximize the number of EVs interacting with the SLBs. The flow was then stopped and the systems were left to equilibrate for approximately 1 h before recording the frequency shift values. The results reported in the manuscript were obtained by taking the average of the values recorded from the 5th, 7th, 9th and 11th harmonics at specific times (see Fig. 1), while the error bars refer to the standard deviation of the four harmonics.

2.6. CLSM experiments

For the Confocal Laser Scanning Microscopy (CLSM) experiments, liposomes and EVs were respectively labelled with two different fluorescent probes (0.1 mol%), characterized by well-separated emission spectra. Fluorescent liposomes and EVs were obtained by incubating the vesicle dispersions overnight with β-Bodipy TM FL C12-HPLC (emission wavelength 512 nm, Thermofisher) and 18:1 Cyanine-5-Phosphatidylethanolamine (Cy5, emission wavelength 663 nm, Avanti Polar Lipids) dry films, respectively. The SLBs were obtained by depositing 100 μl of a 0.1 M NaCl dispersion containing the respective liposomes (at a lipid concentration of 0.5 mg/ml) in three different Borosilicate CLSM wells. Vesicle rupture and SLB formation were then achieved via osmotic shock by gently rinsing the sample with Milli-Q water. To avoid the presence of intact vesicles in the wells, each sample was further rinsed 15 times with MilliQ water. Finally, EVs were injected into the wells from the top using a micropipette. A Leica CLSM TCS SP8 confocal microscope was used to probe the EV-SLB interaction. The fluorescent β-Bodipy probe was excited at 488 nm and its emission was collected in the range 498 −530 nm with a photomultiplier tube (PMT), while Cy5 was excited at a wavelength of 633 nm and collected in the 650 −700 nm range. Images were taken at a resolution of 512 × 512 pixels, after leaving the systems (SLBs or SLBs with EVs) equilibrating for approximately 1 h. Leica Application Suite X (LAS X) software was used to create three-dimensional reconstructions of the z-stacks.

2.7. Theoretical modelling

As is further discussed in the Results and Discussion section, we numerically solved the PB equation (4) for two planar surfaces separated by a distance D under the assumption of constant surface charge density, which is typically an accurate choice for colloidal systems that do not possess a strong propensity to charge regulate through titration of surface groups or adsorption of charged species [32]. This leads to the boundary conditions $\frac{d\psi}{dx}\big|_{x=0} = \frac{\sigma_{SLB}}{\varepsilon_0\varepsilon_r}$ and $\frac{d\psi}{dx}\big|_{x=D} = -\frac{\sigma_{EV}}{\varepsilon_0\varepsilon_r}$, where $\psi(x)$ is the electrostatic potential, σ_{SLB} and σ_{EV} are the SLB and EV surface charge densities, and $\varepsilon_0\varepsilon_r$ is the solvent permittivity. For the SLB surface charge density, we used the estimated values of σ_{SLB} shown in Table 1, calculated using Eq. (3). For the EVs, the surface charge density was adjusted to fit measured adsorption data from CLSM, as described in Results and Discussion. We numerically integrated the PB equation to give the potential profile $\psi(x)$, which can be directly translated into the osmotic pressure, Π, between the two planar surfaces according to [33]

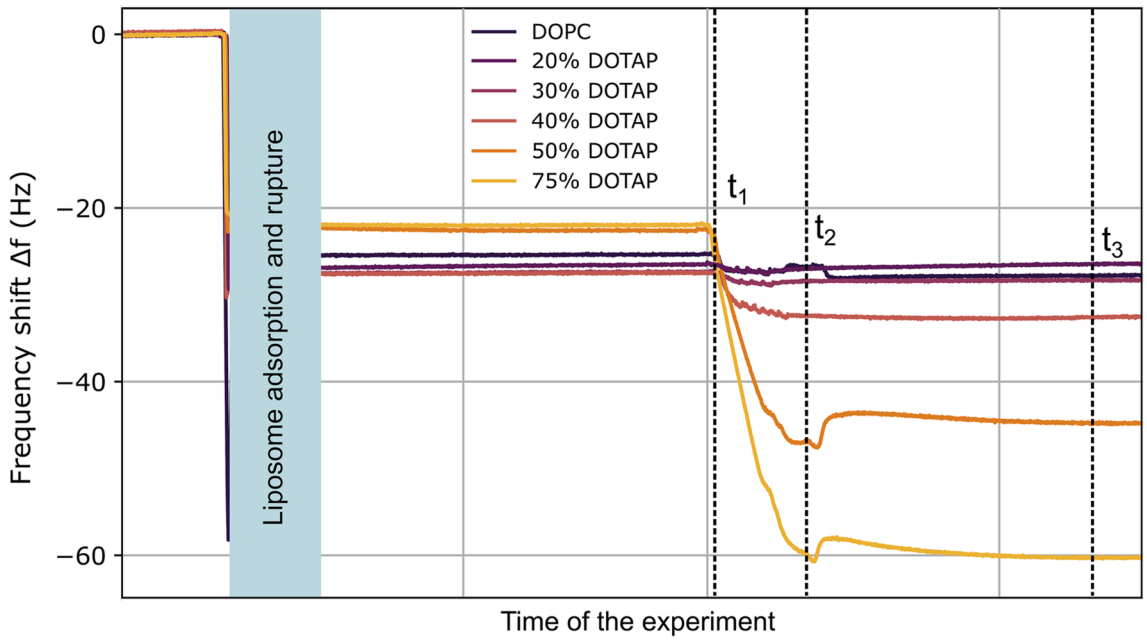

Fig. 1. Representative frequency shifts Δf corresponding to the 5th harmonic for the SLB-EV systems with various SLB compositions, as indicated. The SLB formation is described by the first plateau after the starting baseline, followed by EV injection at t_1. The flow was stopped at t_2, leaving the system to equilibrate until t_3, where the Δf values were recorded.

Table 1
Lipid compositions, measured ζ potential and expected SLB surface charge densities calculated from the lipid compositions of the studied model liposomes.

Liposome composition	Measured ζ potential (mV)	Calculated surface charge density σ(C/m^2)
Pure DOPC	-0.9 ± 0.3	0.00
DOTAP 20%	18 ± 1	0.051
DOTAP 30%	24 ± 2	0.077
DOTAP 40%	27 ± 1	0.103
DOTAP 50%	30 ± 1	0.130
DOTAP 75%	32.1 ± 0.9	0.197
EVs	-7.7 ± 0.9	−0.0094*

*σ_{EV} was adjusted to match the measured EV adsorption as described in Results and Discussion.

$$\Pi = -\frac{e^2 c_0}{k_B T \kappa^2}\left(\frac{d\psi}{dx}\right)^2 + 2k_B T c_0\left(\cosh\left(\frac{e\psi}{k_B T}\right) - 1\right), \tag{1}$$

where e is the elementary charge, κ the inverse Debye screening length, $c_0 = 150$ mM the bulk salt concentration, and $k_B T$ the thermal energy, where we used $T = 298$ K. It should be noted that the right-hand-side of Eq. (1) is independent of x, since the osmotic pressure is uniform across the gap. Integrating the osmotic pressure as a function of the gap distance D yields an expression of the interaction free energy per unit area $A_{PP}(D)$ between the two plates. We then used the Derjaguin approximation [13] to account for the spherical shape of the EV, yielding the sphere-plane force

$$F_{SP}(D) = 2\pi R_0 A_{PP}(D), \tag{2}$$

where R_0 is the EV radius which we set equal to the average hydrodynamic radius of 94.5 nm, as measured from DLS experiments. Finally, numerically integrating the force F_{SP} with respect to D once more yields the electrostatic interaction free energy $A_{El}(D)$ between the planar SLB and spherical EV.

3. Results and discussion

3.1. Characterization of EV and SLB electrostatic properties

Due to their composition, EVs generally possess a weakly negative ζ potential, indicating a net negative surface charge density of their lipid membrane [34]. In our milk EV sample, the measured ζ potential was -7.7 ± 0.8 mV. DLS measurements showed a relatively monodisperse size distribution, with an average EV hydrodynamic radius of $R_0 = 95 \pm 1$ nm and a polydispersity index (PDI) of 0.218 ± 0.029. The ζ potential and size measurements were performed in PBS buffer, corresponding to an inverse Debye screening length of $\kappa = 1.26 \times 10^9$ m^{-1}. Nanoparticle Tracking Analysis (NTA) was furthermore used to measure the vesicle size and concentration, yielding an average vesicle radius of 76 ± 3 nm with a standard deviation of 21 nm, corresponding to an approximate PDI of 0.076, and an EV concentration of 1.84×10^{11} particles per ml (Figure S2). The discrepancy in the EV radii measured from NTA and DLS is expected since the latter technique is biased towards larger particles that scatter light more intensely. For further experimental details, we refer to Materials and Methods and Supplementary Information (SI).

The SLBs were prepared with different DOPC/DOTAP ratios to reveal how electrostatics influences vesicle-membrane interactions. Since DOTAP is positively charged and DOPC is neutral at the studied pH value, we thus obtained synthetic membranes with a controllable surface charge density. Table 1 reports all the liposome compositions used to produce the studied SLBs. As expected, the magnitude of the liposome ζ potential increases with the concentration of DOTAP. The theoretical SLB surface charge density σ_{SLB}, also presented in Table 1, was then calculated from the lipid composition and the approximate headgroup areas of the two lipid species, assuming that each DOTAP molecule carries a single elementary charge regardless of the membrane composition. The latter is a reasonable assumption given that the charge on DOTAP is not titratable; therefore, we do not expect the SLBs to possess a strong ability to regulate their charge in response to changes in its electrostatic environment, *i.e.*, the lipid composition or the ionic strength. The resulting expression for σ_{SLB} is given by

$$\sigma_{SLB} = \frac{e\phi_{DOTAP}}{\phi_{DOPC}a_{DOPC} + \phi_{DOTAP}a_{DOTAP}}, \quad (3)$$

where ϕ_{DOPC} and ϕ_{DOTAP} are the molar fractions of the respective lipid constituents, e is the electron charge, and a_{DOPC} and a_{DOTAP} the headgroup areas of the lipid molecules, taken to be 63.3 Å^2 and 60.4 Å^2, respectively [35]. Since DOPC and DOTAP are miscible and form homogeneous bilayers for most of the studied concentrations [36], we treat the formed SLBs as homogeneously charged surfaces with uniform surface charge density σ_{SLB}. The size range and polydispersity of the liposomes, as measured by Dynamic Light Scattering (DLS) are presented in SI and were furthermore essentially found to be independent of the lipid composition.

3.2. Measurement of EV adsorption through QCM-D

We first used QCM-D to study the adsorption of EVs onto SLBs of varying surface charge density, as reported in Table 1. To form the SLBs, liposomes with different DOPC/DOTAP ratios were injected into the QCM-D flow chamber. Due to mutual interaction and crowding on the sensor surface, the liposomes eventually ruptured and fused, forming uniform SLBs. To promote the rupture of still intact vesicles, milliQ water was flushed through the cell in a second step to create the osmotic imbalance needed to destabilize and rupture the remaining vesicles. The successful formation of continuous SLBs uniformly covering the entire sensor surface is confirmed by the frequency shift (Δf) values displayed in Fig. 1, ranging from 20 to 30 Hz [37], together with the negligible shifts in the dissipation signals (ΔD) relative to the clean crystal (SI) [38–39]. Since the differently charged liposomes adsorbed and formed SLBs according to different mechanisms (*e.g.*, adsorption to the substrate, vesicle rupture, and fusion) and time frames, the parts of the curves describing these phenomena have been omitted from Fig. 1 in order to better compare the differences in the interaction between EV and the various SLBs; the full QCM-D plots including the adsorption and rupture phases are instead reported in Fig. S3. The small differences between the Δf values at the first plateau, corresponding to the point when the equilibrated SLBs covered the entire sensor surface, can be attributed to both their differing compositions and the variability between different experiments.

After SLB equilibration EVs were injected into the flow chamber, as indicated by t_1 in Fig. 1. The sudden drop in Δf indicates a significant interaction of the EVs with the SLB surface. The extent of the Δf drop strongly depends on the surface charge density of the SLBs: while the pure DOPC SLB, formed from liposomes characterized by a weakly negative ζ potential, displays a negligible frequency drop, the highly positively charged 75% DOTAP SLB features the highest Δf, indicating significant EV adsorption. After the injection phase, the flow was stopped (marked by t_2 in Fig. 1) and the EVs were left to equilibrate with the SLBs for one hour until a new stable plateau in Δf was reached (point t_3 in Fig. 1). The steady-state Δf values were recorded at t_3 and were used for evaluating the EV adsorption at equilibrium. The bar plot in Fig. 2 reports the difference in the Δf and ΔD values between t_3 (after equilibration) and t_1 (before EV injection) for the different SLB compositions and gives an indication of the amount of EVs adsorbed onto the respective SLB. The results confirm that EV adsorption strongly depends on the SLB surface charge density: for SLBs with DOTAP fractions lower than 40%, EV adsorption is negligible with no significant difference in Δf compared to the pure DOPC bilayer. EV adsorption starts to occur for SLBs with a DOTAP percentage of 40% and then increases sharply with the concentration of the cationic phospholipid. After EV adsorption, the dissipation signals increase proportionally to the DOTAP concentration, eventually reaching ΔD values in the 9 −11.5 ppm range (Figs. 2 and S3); such large dissipation shifts suggest the formation of a layer of intact EVs oscillating out of phase with respect to the underlying SLB. This interpretation is further strengthened by the dependency of both Δf and ΔD on the DOTAP concentration and by the spreading of the different

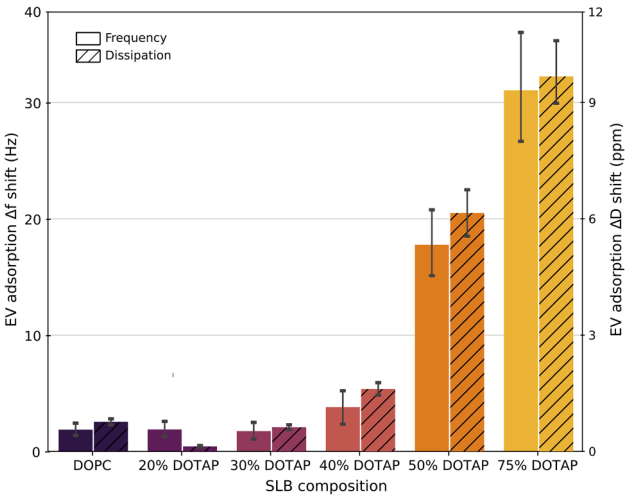

Fig. 2. Average QCM-D frequency and dissipation shifts (Δf and ΔD, respectively) due to EV adsorption on the various SLBs, as indicated. The shifts are measured as the difference between the Δf or ΔD values recorded at times t_3 and t_1 illustrated in Fig. 1. The plotted values represent an average over the 5th, 7th, 9th, and 11th harmonics, and error bars indicate the standard deviation of the four values.

harmonics (Fig. S3). If instead EVs had ruptured and merged with the SLB, the frequency and dissipation shifts should be similar for all membrane compositions where adsorption occurs. More specifically, Δf would plateau at a constant value and ΔD would be close to zero, with only small differences between the different harmonics. Even though recent studies [26–27] have demonstrated EV-SLB fusion after adsorption, these have relied on more specific interactions, respectively the adsorption to the boundaries between liquid-ordered and liquid-disordered phases [26] and antibody-mediated attractive interactions [27]. In contrast, we expect our system to lack any strong attractive interactions apart from generic electrostatic and van der Waals interactions, which have previously been shown insufficient to induce membrane fusion [40].

Extending this qualitative interpretation of QCM-D results to properly account for the formation of multilayered viscoelastic systems, such as vesicles adsorbed on top of soft SLBs, is however highly complex. Specifically, translating the obtained Δf values into more physical parameters such as adsorbed mass is not straightforward, since, among other things, the results will be influenced by dissipative phenomena related to the water trapped within the vesicles and between the multiple layers [41–42]. While the Voigt model [41] could in principle be used for modelling the adsorption of such viscoelastic soft layers, this model requires *a priori* knowledge of properties such as the density and viscosity of the adsorbed layers, which in this case are both unknown and highly dependent on the morphology of the adsorbed EVs.

3.3. CLSM analysis of EV-SLB interactions

To gain further insight into EV adsorption, interaction, and organization on the surface of the charged SLBs, we performed CLSM experiments on the same SLB-EV systems as analyzed by QCM-D. The experiments focused on three different DOPC/DOTAP SLB configurations as substrates. More precisely, we studied (i) pure DOPC as a negative control for EV adsorption (ii) 40% DOTAP, and (iii) 50% DOTAP, where the latter two represent the SLB compositions between which the QCM-D experiments recorded the most dramatic change in EV adsorption. Fig. S4 displays representative images of the obtained SLBs and confirms the formation of homogeneous, fluorescent lipid bilayers covering the entire surface for all three lipid mixtures.

After a 30-minute equilibration time, 100 μl of EV solution at the

same concentration used in the QCM-D experiments was added to the sample wells and images were collected at specific time intervals. Fig. 3 reports representative top-view 2D images of the SLB-EV systems, collected after 1 h of incubation after EV injection. The green channel accounts for the fluorescence signal from the SLBs (left column), while the fluorescence from the EVs is displayed in red (centre column). As a result, the superposition of the two channels (right column) in areas where the green and red fluorescence intensities are comparable appears yellow. The results demonstrate that, after one hour of incubation, no EVs had visibly adsorbed on the pure DOPC SLB (top row). Moreover, Movie S7 shows that even those EVs that approach the DOPC SLB surface do not adsorb but are free to move away from the SLB, confirming the negligible adsorption recorded in the corresponding QCM-D experiment. EVs start to adsorb on the 40% DOTAP SLB, forming a few localized fluorescent aggregates (Fig. 3 and S5). EV adsorption on the 50% DOTAP SLB (centre column, bottom row in Fig. 3) is however significantly higher: after one hour, the 50% DOTAP SLB is characterized by an intense red fluorescence signal across the whole surface, indicating strong adsorption of EVs compared to the limited adsorption on the 40% DOTAP SLB. To ensure that the fluorescence signal is solely due to adsorbed EVs rather than to free dye adsorption, we performed control experiments on the same SLB systems without EVs but with the red dye Cy5 present. As shown in Fig. S6, the red fluorescence signal effectively vanishes in the absence of EVs for all three SLBs, showing that the signal is indeed due to EV adsorption.

The CLSM results thus highlight the strong attractive interaction between EVs and the more highly charged 50% DOTAP SLB and support our interpretation of the QCM-D results. Notably, the combined fluorescence signal from the 50% DOTAP SLB + EVs system (Fig. 3 right column, bottom row) is still mostly saturated by the green fluorescence from the underlying SLB, meaning that the adsorbed EVs did not rupture and form a tightly packed lipid bilayer. Fig. S5 furthermore shows 3D CLSM images of the adsorbed EVs on the 40% and 50% DOTAP SLBs; in the latter case, the image confirms that EVs adsorb on the entire SLB, even forming large aggregates in specific regions, but without rupturing and merging into a flat lipid bilayer. To address the mechanistic details of the EV-SLB interaction and obtain a more thorough understanding of the colloidal forces driving each single vesicle to adsorption, we will in

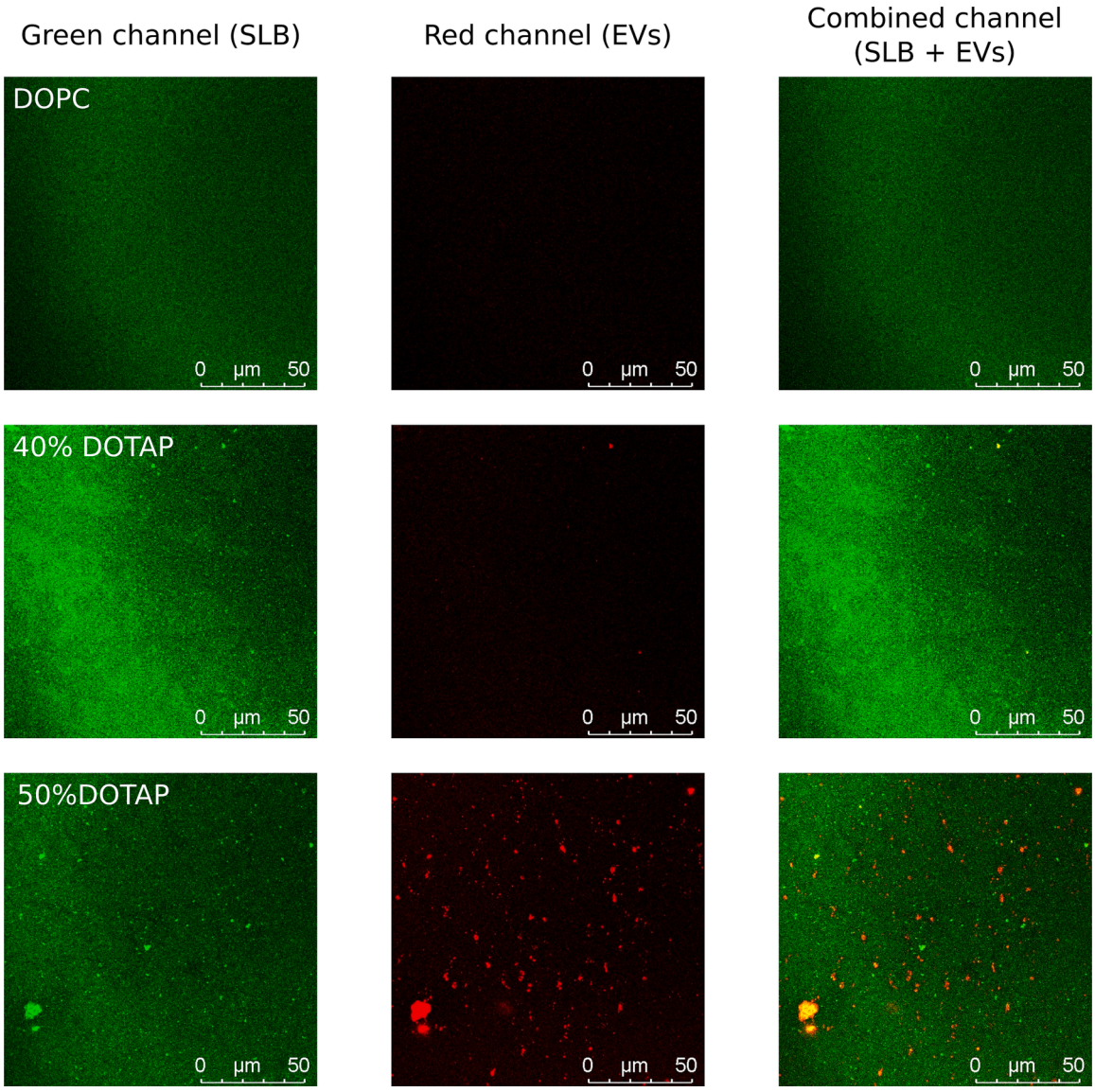

Fig. 3. Representative top-view 2D CLSM images of the probed SLB-EV systems: DOPC (top row), 40% DOTAP (middle row) and 50% DOTAP (bottom row), collected 1 h after EV injection. The green and red channels respectively report the fluorescent intensities of SLBs (left column) and EVs (centre column). The superposition of the two channels is shown in the right column. (For interpretation of the references to colour in this figure legend, the reader is referred to the web version of this article.)

the next section formulate a theoretical model for the interaction energy between the SLB and the EVs.

3.4. Theoretical modelling of EV-SLB interaction

To verify that the electrostatic interaction between EVs and oppositely charged SLBs is indeed the dominant driving force for EV adsorption observed in microscopy and QCM-D, we built a semi-quantitative description based on the Poisson-Boltzmann (PB) equation describing the electrostatic interactions [43]. Unlike in standard DLVO theory, we consider a full nonlinear PB description of the interaction between *unequally* charged particles, which furthermore makes it necessary to solve the PB equation without any symmetry about the midplane. In addition, we included the effect of short-ranged, repulsive "steric-hydration" forces that are known to generically act between hydrated lipid bilayers.

Within the PB framework, two oppositely charged macroions or surfaces immersed in a salt solution will attract at long range due to the favorable free energy associated with releasing the counterions into the bulk solution as the two surfaces approach each other [33,43]. If the two surface charge densities σ_1 and σ_2 are equal and opposite (*i.e.*,$\sigma_1 = -\sigma_2$), this attraction will persist monotonically down to close contact, where the two surfaces will neutralize each other completely and release all counterions into the bulk. In the typical case where $\sigma_1 \neq -\sigma_2$, the attraction will instead change into a repulsion at the separation where all "excess" counterions have been released into the bulk; the layer of remaining counterions that neutralize the total charge $\sigma_1 + \sigma_2$ of the two surfaces is then compressed as the surfaces approach further, leading to a repulsive entropic force [33]. Thus, within the PB framework, we expect an electrostatic interaction free energy with a well-defined minimum at intermediate separations, whose depth and location depend on the respective surface charge densities and the salt concentration.

We model a single EV as a negatively charged sphere with constant and homogeneous surface charge density σ_{EV}, while the SLB is modelled as a rigid flat plane with corresponding charge density σ_{SLB}. For a monovalent (1:1) salt solution at bulk concentration c_0, the nonlinear PB equation for two flat parallel surfaces reads

$$\frac{d^2\psi}{dx^2} = \frac{2ec_0}{\varepsilon_0\varepsilon_r}\sinh\left(\frac{e\psi}{k_BT}\right). \tag{4}$$

Here $\psi(x)$ is the electrostatic potential, $x \in [0, D]$ the position along the surface normal, ε_0 is the vacuum permittivity, ε_r the relative dielectric permittivity of water, and k_BT the thermal energy. The SLB surface charge densities σ_{SLB} for the various compositions were calculated using Eq. (3) and are listed in Table 1. The EV surface charge density σ_{EV} is more difficult to estimate *a priori*; we therefore manually adjusted this value to the one that gave the best agreement with the experimental estimate of the adsorbed amount of EVs for the 50% DOTAP system, as discussed below and shown in Fig. 5, yielding a value of $\sigma_{EV} = -0.0094$ Cm^{-2}. By numerically integrating Eq. (4) as described in Materials and Methods, we obtained the electrostatic free energy $A_{El}(D)$ between the spherical EV and the flat SLB, where D is the minimum separation between the two surfaces. The electrostatic interaction curves are plotted in Fig. 4a, showing that these alone indeed lead to a non-monotonic behavior, with a free energy minimum whose depth is roughly independent of the SLB charge density (controlled by the DOTAP fraction) but whose position gradually moves towards larger separations as the DOTAP content is increased.

For lipid bilayers in aqueous solution, it is well-established that a short-ranged, repulsive force acts to prevent adsorption and adhesion due to attractive van der Waals forces, even in the absence of electrostatic stabilization mechanisms [13]. While the mechanistic origin of this "steric-hydration" force is still debated, it is empirically well characterized as an exponentially decaying interbilayer pressure, $P_{SH} = P_0\exp(-D/D_0)$, with a decay length D_0 on the order of 1 nm. Since we cannot easily measure the force curve between our mixed DOPC/DOTAP

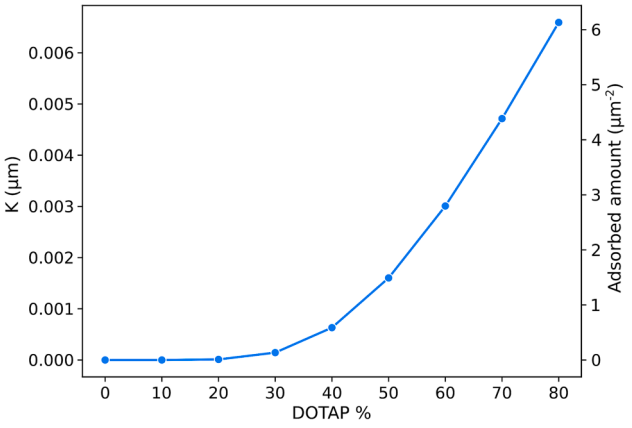

Fig. 5. Calculated values of the equilibrium constant K for EV adsorption (left ordinate axis) and the adsorbed amount Γ (right axis) as a function of the SLB composition, as calculated from Eq. (6) and using the measured bulk concentration $c_{EV} = 9.3 \times 10^8$ ml^{-1}.

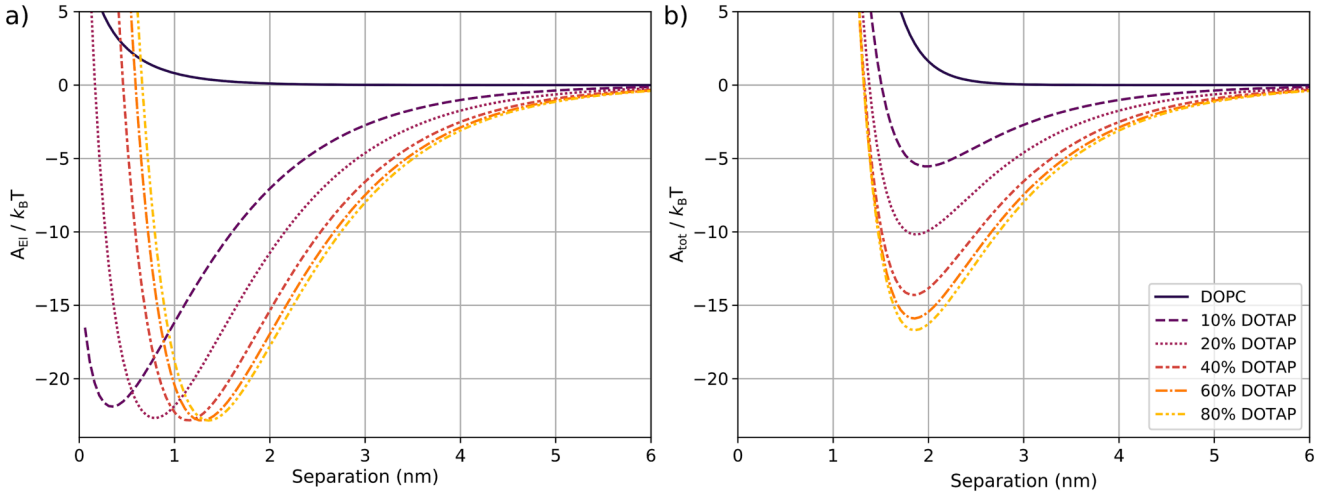

Fig. 4. Interaction free energy for different SLB compositions, including the effect of (a) electrostatic forces alone and (b) electrostatic forces and short-ranged steric-hydration forces as given by Eq. (5) with $A_0 = 4500k_BT$ and $D_0 = 0.25$ nm.

bilayers and the complex EV surface, we instead used the parameters $D_0 = 0.25$ nm and $P_0 = 5 \times 10^8$ N/m^2 previously measured for the interaction between uncharged lecithin bilayers [40]. Importantly, this empirically measured short-range force represents the *total* force acting between two SLBs, and thus implicitly also includes the short-range part of van der Waals attractions and any other non-electrostatic interactions acting between the SLBs. Applying the Derjaguin approximation and integrating the pressure twice, we obtain the repulsive interaction between a sphere and a plane:

$$A_{\mathrm{SH}}(D) = 2\pi R_0 D_0^2 P_0 \exp\left(-\frac{D}{D_0}\right) \equiv A_0 \exp\left(-\frac{D}{D_0}\right), \tag{5}$$

where R_0 is the EV radius and our parameter values yield $A_0 = 4500 k_B T$. Due to this large prefactor, the steric-hydration force will be dominant below separations of $D \approx 3$ nm, beyond which the attractive van der Waals becomes dominant. This long-ranged tail of the van der Waals force is however expected to be small, and we thus neglected it in our description. In Fig. 4b, we plot the total interaction energy $A_{\mathrm{Tot}}(D) = A_{\mathrm{El}} + A_{\mathrm{SH}}$ for SLBs with DOTAP fractions from 0 to 80%. As can be seen, the combination of the two forces makes the attractive minimum change its depth significantly with SLB charge density, while remaining at a roughly constant separation of $D \approx 2$ nm. This indicates that we should expect a monotonically increasing EV adsorption with increasing DOTAP fraction.

To further quantify this observation, we note that the equilibrium constant K for adsorption of EVs on the SLB surface can be related to the interaction free energy *via* [43]

$$K \simeq \int_0^\infty \left[\exp\left(-\frac{A_{\mathrm{Tot}}(D)}{k_B T}\right) - 1\right] dD. \tag{6}$$

In Fig. 5 (left ordinate axis), we report the calculated values of K from Eq. (6) as a function of the SLB composition. The reported values clearly show that our model predicts an electrostatically induced adsorption starting from DOTAP fractions above 30%, in excellent agreement with our experimental results.

The modelling also shows that the adsorbed amount is expected to increase continuously with the DOTAP fraction, in accordance with the observed frequency shifts in QCM-D. This fact is not obvious *a priori*, as a simple picture based on the electrostatic interaction alone would lead to a sharp initial increase in adsorbed amount already for small DOTAP fractions, followed by an essentially constant plateau. This can be seen by the fact that the depth and width of the free energy minimum in the purely electrostatic picture (Fig. 4a) are essentially constant beyond 10% DOTAP, a picture that changes qualitatively when the effect of short-ranged repulsive forces is added (Fig. 4b).

The calculated equilibrium constant K can furthermore be related to the number of adsorbed EVs per unit area, Γ, *via* its definition $\Gamma = K c_{\mathrm{EV}}$, where $c_{\mathrm{EV}} \approx 9.3 \times 10^8$ ml^{-1} is the measured bulk EV concentration after adjusting for the different dilutions. We experimentally estimated Γ from the CLSM image at 50% DOTAP (Fig. 3, bottom row, center panel) by measuring the total area of the bright spots in the image, using the software *Gwyddion* [44]. The number of adsorbed EVs per unit area was obtained by dividing the total area by the projected area πR_0^2 of a single EV and by the total image area, yielding $\Gamma \approx 1.49\,\mu\mathrm{m}^{-2}$. Obviously, this estimate is highly approximate and potentially also affected by the fact that the bare size of individual EVs is below the CLSM resolution limit (250 nm); nevertheless, we believe that it is accurate enough to perform a semiquantitative comparison between the PB modelling and experimental results. The experimentally estimated value of Γ was then used to adjust the unknown EV surface charge density to $\sigma_{\mathrm{EV}} = -0.0094$ Cm^{-2}. This value corresponds to an EV surface potential of $\psi_0 \approx \sigma_{\mathrm{EV}}/(\varepsilon_0 \varepsilon_r \kappa) = -10.6$ mV, with κ being the inverse Debye screening length, and where the linear relation between surface potential and surface charge is accurate for low potentials such as those measured for EVs. Just as expected, the estimated value of the surface potential has the same sign and somewhat larger magnitude than the measured EV ζ potential of -7.7 mV (see Table 1), since the ζ potential is measured in the slip plane of the double layer where part of the surface charge has been screened.

The fact that we can obtain an excellent agreement between theoretical modelling and experimental results using reasonable parameter values indicates that EV adsorption is indeed controlled by an interplay between the long-ranged attractive and short-ranged repulsive forces acting in the system. The theoretical results furthermore explain the experimental observation that EVs will start to adsorb onto the SLB above a composition of approximately 40% DOTAP and that they do not reach adhesive contact with the SLB, but rather remain adsorbed at some finite distance outside the membrane. This is in accordance with previous experimental results [40] indicating that electrostatic interactions are typically not sufficient to induce fusion, likely due to the repulsive barrier induced by compression of the remaining counterions. In this picture, fusion will only occur when deformations within the EV membrane and SLB expose the hydrocarbon groups and hence give rise to attractive hydrophobic interactions.

4. Conclusion

The results presented here demonstrate that electrostatic interactions can be used to control the adsorption of EVs onto charged lipid membranes. More precisely, we have shown that EVs readily adsorb, without merging with the SLB, onto membranes possessing opposite surface charge densities σ higher than a specific threshold value. When adsorption occurs, its extent is found to be roughly proportional to σ. Modelling the system within the framework of nonlinear Poisson-Boltzmann theory confirms the experimental results and shows that electrostatic interactions are indeed sufficient to cause the irreversible binding of EVs to charged SLBs, but prevent attraction down to molecular contact due to the remaining counterions. This suggests that electrostatic interactions may play a role in vesicle-mediated intercellular communication, since they are capable of causing irreversible binding of EVs with the charged sites of the cell membrane. However, these forces alone are likely not sufficient to account for EV fusion or uptake, phenomena where other types of interactions come into play. This is in agreement with previous works that documented EV fusion due to either the energetically favorable conditions encountered along the host membrane phase boundaries [26] or antibody-mediated attractive interactions [27]. Taken together, our findings highlight the fundamental role played by surface charge in the interaction of EVs at the nanoscale, adding to the knowledge about their stability and binding propensity to lipid interfaces. Our work furthermore demonstrates that the interactions of molecularly complex systems such as EVs can be successfully characterized using simple theoretical descriptions derived from colloidal science. Given the growing interest in employing EVs for numerous biomedical applications, our results are of potential interest for developing efficient EV immobilization strategies necessary for controlling and manipulating systems based on these natural lipid-based nanocarriers.

CRediT authorship contribution statement

Andrea Ridolfi: Conceptualization, Methodology, Investigation, Writing – original draft, Writing – review & editing. **Jacopo Cardellini:** Investigation, Methodology. **Fatlinda Gashi:** Investigation. **Martijn J. C. van Herwijnen:** Investigation, Resources, Writing – review & editing. **Martin Trulsson:** Formal analysis, Writing – review & editing. **José Campos-Terán:** Investigation, Writing – review & editing. **Marca H. M. Wauben:** Resources, Writing – review & editing. **Debora Berti:** Conceptualization, Writing – review & editing, Supervision. **Tommy Nylander:** Conceptualization, Writing – review & editing, Supervision. **Joakim Stenhammar:** Conceptualization, Methodology, Writing – original draft, Writing – review & editing, Supervision.

Declaration of Competing Interest

The authors declare that they have no known competing financial interests or personal relationships that could have appeared to influence the work reported in this paper.

Data availability

Data will be made available on request.

Acknowledgements

JS acknowledges enlightening discussions with Håkan Wennerström. We thank Marije Kleinjan (Utrecht University, Department of Biomolecular Health Sciences, The Netherlands) for technical support in preparing milk EV samples and Valentina Moccia (Department of Comparative Biomedicine and Food Science, University of Padua, Italy) for technical support in the NTA characterization. This work has been supported by the European Community through the evFOUNDRY project (H2020-FETopen, ID: 801367).

Appendix A. Supplementary data

Supplementary data to this article can be found online at https://doi.org/10.1016/j.jcis.2023.07.018.

References

[1] L. Sapir, S. Tzlil, Talking over the extracellular matrix: how do cells communicate mechanically? Semin. Cell Dev. Biol. 71 (2017) 99–105.
[2] M. Mittelbrunn, F. Sánchez-Madrid, Intercellular communication: diverse structures for exchange of genetic information, Nat. Rev. Mol. Cell Biol. 13 (2012) 328–335.
[3] K.C. Vickers, A.T. Remaley, Lipid-based carriers of microRNAs and intercellular communication, Curr. Opin. Lipidol. 23 (2012) 91–97.
[4] B. György, et al., Membrane vesicles, current state-of-the-art: emerging role of extracellular vesicles, Cell. Mol. Life Sci. 68 (2011) 2667–2688.
[5] M. Tkach, C. Théry, Communication by extracellular vesicles: where we are and where we need to go, Cell 164 (2016) 1226–1232.
[6] G. Camussi, M.C. Deregibus, S. Bruno, V. Cantaluppi, L. Biancone, Exosomes/microvesicles as a mechanism of cell-to-cell communication, Kidney Int. 78 (2010) 838–848.
[7] G. Berumen Sánchez, K.E. Bunn, H.H. Pua, M. Rafat, Extracellular vesicles: mediators of intercellular communication in tissue injury and disease, Cell Commun. Signal. CCS 19 (2021) 104.
[8] G. Van Niel, G. D'Angelo, G. Raposo, Shedding light on the cell biology of extracellular vesicles, Nat. Rev. Mol. Cell Biol. 19 (2018) 213–228.
[9] M. Yáñez-Mó, et al., Biological properties of extracellular vesicles and their physiological functions, J. Extracell. Vesicles 4 (2015) 27066.
[10] R. Kalluri, V.S. LeBleu, The biology, function, and biomedical applications of exosomes, Science 367 (2020).
[11] L.A. Mulcahy, R.C. Pink, D.R.F. Carter, Routes and mechanisms of extracellular vesicle uptake, J. Extracell. Vesicles 3 (2014).
[12] K.C. French, M.A. Antonyak, R.A. Cerione, Extracellular vesicle docking at the cellular port: Extracellular vesicle binding and uptake, Semin. Cell Dev. Biol. 67 (2017) 48–55.
[13] J.N. Israelachvili, Intermolecular and surface forces. 151 (2015).
[14] J. Marra, J. Israelachvili, Direct measurements of forces between phosphatidylcholine and phosphatidylethanolamine bilayers in aqueous electrolyte solutions, Biochemistry 24 (1985) 4608–4618.
[15] K. Dimitrievski, B. Kasemo, Influence of lipid vesicle composition and surface charge density on vesicle adsorption events: a kinetic phase diagram, Langmuir 25 (2009) 8865–8869.
[16] K. Dimitrievski, B. Kasemo, Simulations of lipid vesicle adsorption for different lipid mixtures, Langmuir 24 (2008) 4077–4091.
[17] M. Dacic, et al., Influence of divalent cations on deformation and rupture of adsorbed lipid vesicles, Langmuir 32 (2016) 6486–6495.
[18] J.A. Jackman, Z. Zhao, V.P. Zhdanov, C.W. Frank, N.J. Cho, Vesicle adhesion and rupture on silicon oxide: Influence of freeze-thaw pretreatment, Langmuir 30 (2014) 2152–2160.
[19] R.P. Richter, R. Bérat, A.R. Brisson, Formation of solid-supported lipid bilayers: An integrated view, Langmuir 22 (2006) 3497–3505.
[20] A. Ridolfi, et al., Stiffness of fluid and gel phase lipid nanovesicles: weighting the contributions of membrane bending modulus and luminal pressurization, Langmuir 37 (2021) 12027–12037.
[21] A. Ridolfi, et al., AFM-based high-throughput nanomechanical screening of single extracellular vesicles, Anal. Chem. 92 (2020) 10274–10282.
[22] L.A. Clifton, et al., Design and use of model membranes to study biomolecular interactions using complementary surface-sensitive techniques, Adv. Colloid Interface Sci. 277 (2020), 102118.
[23] G.J. Hardy, R. Nayak, S. Zauscher, Model cell membranes: techniques to form complex biomimetic supported lipid bilayers via vesicle fusion, Curr. Opin. Colloid Interface Sci. 18 (2013) 448–458.
[24] T.N. Sut, B.K. Yoon, W.-Y. Jeon, J.A. Jackman, N.-J. Cho, Supported lipid bilayer coatings: Fabrication, bioconjugation, and diagnostic applications, Appl. Mater. Today 25 (2021), 101183.
[25] E. Reimhult, F. Höök, B. Kasemo, Intact vesicle adsorption and supported biomembrane formation from vesicles in solution: influence of surface chemistry, vesicle size, temperature, and osmotic pressure, Langmuir 19 (2003) 1681–1691.
[26] F. Perissinotto, et al., Structural insights into fusion mechanisms of small extracellular vesicles with model plasma membranes, Nanoscale 13 (2021) 5224–5233.
[27] H.-Y. Liu, et al., Rapid capture of cancer extracellular vesicles by lipid patch microarrays, Adv. Mater. 33 (2021) 2008493.
[28] M.-L. Ainalem, et al., DNA binding to zwitterionic model membranes, Langmuir ACS J. Surf. Colloids 26 (2010) 4965–4976.
[29] D. McLoughlin, et al., Surface complexation of DNA with insoluble monolayers. Influence of divalent counterions, Langmuir 21 (2005) 1900–1907.
[30] T.M. Podgornik, D. Andelman, Rudolf., Charged Membranes: Poisson-Boltzmann Theory, The DLVO Paradigm, and Beyond. Handbook of Lipid Membranes, (CRC Press, 2021.
[31] M.I. Zonneveld, et al., Human milk extracellular vesicles target nodes in interconnected signalling pathways that enhance oral epithelial barrier function and dampen immune responses, J. Extracell. Vesicles 10 (2021) e12071.
[32] Y. Avni, D. Andelman, R. Podgornik, Charge regulation with fixed and mobile charged macromolecules, Curr. Opin. Electrochem. 13 (2019) 70–77.
[33] D. Ben-Yaakov, D. Andelman, Revisiting the Poisson-Boltzmann theory: charge surfaces, multivalent ions and inter-plate forces, Phys. Stat. Mech. Its Appl. 389 (2010) 2956–2961.
[34] G. Midekessa, et al., Zeta potential of extracellular vesicles: toward understanding the attributes that determine colloidal stability, ACS Omega 5 (2020) 16701–16710.
[35] A. Zidovska, H.M. Evans, A. Ahmad, K.K. Ewert, C.R. Safinya, The role of cholesterol and structurally related molecules in enhancing transfection of cationic liposome−DNA complexes, J. Phys. Chem. B 113 (2009) 5208–5216.
[36] I. Koltover, T. Salditt, C.R. Safinya, Phase diagram, stability, and overcharging of lamellar cationic lipid–DNA self-assembled complexes, Biophys. J. 77 (1999) 915–924.
[37] R. Richter, A. Mukhopadhyay, A. Brisson, Pathways of Lipid Vesicle Deposition on Solid Surfaces: A Combined QCM-D and AFM Study, Biophys. J . 85 (2003) 3035–3047.
[38] E. Reimhult, F. Höök, B. Kasemo, Vesicle adsorption on SiO2 and TiO2: dependence on vesicle size, J. Chem. Phys. 117 (2002) 7401–7404.
[39] E. Reimhult, B. Kasemo, F. Höök, Rupture pathway of phosphatidylcholine liposomes on silicon dioxide, Int. J. Mol. Sci. 10 (2009) 1683–1696.
[40] C.A. Helm, J.N. Israelachvili, P.M. McGuiggan, Role of hydrophobic forces in bilayer adhesion and fusion, Biochemistry 31 (1992) 1794–1805.
[41] M.V. Voinova, M. Rodahl, M. Jonson, B. Kasemo, Viscoelastic acoustic response of layered polymer films at fluid-solid interfaces: continuum mechanics approach, Phys. Scr. 59 (1999) 391–396.
[42] F. Höök, et al., Variations in coupled water, viscoelastic properties, and film thickness of a Mefp-1 protein film during adsorption and cross-linking: a quartz crystal microbalance with dissipation monitoring, ellipsometry, and surface plasmon resonance study, Anal. Chem. 73 (2001) 5796–5804.
[43] D. Fennell Evans, & Wennerström, H, Where Physics, Chemistry, Biology, and Technology Meet, The Colloidal Domain, 1999.
[44] D. Nečas, P. Klapetek, Gwyddion: An open-source software for SPM data analysis, Cent. Eur. J. Phys. 10 (2012) 181–188.